Available online at www.sciencedirect.com

SCIENCE DIRECT

Developmental Biology 278 (2005) 86–102

DEVELOPMENTAL BIOLOGY

www.elsevier.com/locate/ydbio

Apoptosis and proliferation in developing, mature, and regressing epibranchial placodes

Stefan Washausen[a], Bastian Obermayer[a], Guido Brunnett[b], Hans-Jürg Kuhn[a], Wolfgang Knabe[a,*]

[a]*Department of Anatomy/Embryology, Georg August University, Kreuzbergring 36, D-37075 Göttingen, Niedersachsen, Germany*
[b]*Department of Informatics, Technical University, 09107 Chemnitz, Germany*

Received for publication 18 September 2004, revised 23 October 2004, accepted 25 October 2004
Available online 18 November 2004

Abstract

Epibranchial placodes and rhombencephalic neural crest provide precursor cells for the geniculate, petrosal, and nodose ganglia. In chick embryos and in *Tupaia belangeri*, apoptosis in rhombomeres 3 and 5 helps to select premigratory precursor cells and to segregate crest cell streams derived from the even-numbered rhombomeres. Much less is known about the patterns and functions of apoptosis in epibranchial placodes. We found that, in *Tupaia belangeri*, combined anlagen of the otic placode and epibranchial placode 1 transiently share a primordial low grade thickening with post-otic epibranchial placodes. Three-dimensional reconstructions reveal complementary, spatially, and temporally regulated apoptotic and proliferative events that demarcate the otic placode and epibranchial placode 1, and help to individualize three pairs of epibranchial placodes in a rostrocaudal sequence. Later, rostrocaudal waves of proliferation and apoptosis extend from dorsal to ventral parts of the placodes, paralleled by the dorsoventral progression of precursor cell delamination. These findings suggest a role for apoptosis during the process of neuroblast generation in the epibranchial placodes. Finally, apoptosis eliminates remnants of the placodes in the presence of late invading macrophages.

Keywords: Apoptosis; Proliferation; Epibranchial placodes; Hindbrain; Neural crest; Cranial nerves; Development; 3-D reconstruction; Mammal

Introduction

Epibranchial placodes are serially arranged ectodermal thickenings that develop dorsocaudally adjacent to the branchial membranes. In mammals, three pairs of epibranchial placodes provide sensory neurons for the geniculate, petrosal, and nodose ganglia. Ganglionic glial cells are recruited from the rhombencephalic neural crest (Baker and Bronner-Fraser, 2001; Webb and Noden, 1993). Mechanisms should be in place that coordinate the production, survival, and differentiation of precursor cells in the two distant sources. In fact, in chick embryos (Graham et al., 1993) and in *Tupaia belangeri* (Knabe et al., 2004), large-scale apoptosis of premigratory neural crest cells in rhombomeres 3 and 5 helps to segregate streams of crest cells that emigrate from rhombomeres 1/2, 4, and 6/7. Consequently, crest cell streaming guides axons of placode-derived neurons to the correct afferent location in the hindbrain (Begbie and Graham, 2001; Graham et al., 2004).

Reports on physiologically occurring cell death in the epibranchial placodes are sparse (Adelmann, 1925; Batten, 1957; Sulik et al., 1987; Theiler, 1949). In embryonic mice, highest numbers of apoptotic placodal cells are found in the 33 somite embryo (Sulik et al., 1987). Compared with wildtype embryos, apoptosis in epibranchial placodes or among placode-derived neuroblasts is increased in zebrafish lacking the transcription factor Foxi 1 (Lee et al., 2003), and in embryonic mice exposed to ethanol (Kotch and Sulik, 1992; Sulik et al., 1986), retinoic acid (Sulik et al., 1987), or manipulated by blocking retinoid signal transduction (Wendling et al., 2000). According to Sulik et al. (1987, 1988), the excessive apoptotic loss of cells derived from the

* Corresponding author. Fax: +49 551 397043.
E-mail address: wknabe@gwdg.de (W. Knabe).

0012-1606/$ - see front matter © 2004 Elsevier Inc. All rights reserved.
doi:10.1016/j.ydbio.2004.10.016

trigeminal and epibranchial placodes promotes the development of mandibulofacial dysostosis (Treacher Collins)-like syndromes. On the other hand, Dixon et al. (1997, 2000) state that pathologically increased apoptosis of premigratory neural crest cells is the primary cause of the Treacher Collins syndrome. Taken together, these findings encouraged to test whether physiologically regulated patterns of apoptosis in the epibranchial placodes exist, and whether these patterns are temporally and functionally related with the known rhombomere-specific patterns of apoptosis (Graham et al., 1993; Knabe et al., 2004).

Epibranchial placodes develop within larger areas of thickened branchial surface ectoderm (Baker and Bronner-Fraser, 2000; Bartelmez and Evans, 1926; D'Amico-Martel and Noden, 1983; Müller and O'Rahilly, 1988; Verwoerd and van Oostrom, 1979). The existence of a common primordial thickening for most, if not all cephalic placodes of vertebrates, has been postulated or disputed (Schlosser, 2002). Advancing insights into the molecular mechanisms of placode development suggest that, in fact, "different placodes evolved from a common placodal primordium by successive recruitment of new inducers and target genes" (Schlosser and Ahrens, 2004). Thus, in *Xenopus laevis*, otic and epibranchial placodes as well as lateral line placodes share a common primordial thickening and the expression patterns for many different transcription factors (Schlosser and Ahrens, 2004). Accordingly, in chick embryos, the transcription factor cSox3 is initially expressed throughout the epiblast. From Hamburger Hamilton stage 10 (Hamburger and Hamilton, 1951) onwards, cSox3 is secondarily upregulated in two thickened areas which encompass (1) the otic placode and epibranchial placode 1, and (2) developing epibranchial placode 2 as well as the two vagal epibranchial placodes. Finally, isolated patches of cSox3 demarcate the definitive epibranchial placodes (Ishii et al., 2001).

To comprehensively demonstrate developing epibranchial placodes in their cellular and organismic context, we have established a system that performs three-dimensional reconstructions of small cellular events in large objects (Knabe and Kuhn, 1998; Knabe et al., 2000). This system was stepwise improved (1) by introducing "Huge Image", a scanning system which permits data acquisition from semithin sections at maximum light microscopic resolution (Knabe et al., 2002; Süss et al., 2002), (2) by setting up a procedure that realigns vectorized histological serial sections with the help of external fiducials (Knabe et al., 2002), and (3) by implementing triangulation algorithms for the rapid reconstruction of large internal and external embryonic surfaces (Brunnett et al., 2003). In the past, this system helped to identify bands of apoptotic cells that, probably, forward bilateralization processes of the entire forebrain (Knabe and Kuhn, 1998; Knabe et al., 2000). Additionally, a straightforward sequence of rhombomere-specific apoptotic events was observed in the developing hindbrain of the tree shrew *Tupaia belangeri* (Knabe et al., 2004). Tree shrews are diurnal mammals, and their relationship to primates is under debate (Wible and Zeller, 1994).

The present work investigates, whether and how spatially and temporally regulated patterns of apoptosis and proliferation contribute to the morphogenesis and fate of the epibranchial placodes in *Tupaia belangeri*. Since macrophages may either eliminate apoptotic cells (Rabinovitch, 1995) or induce apoptosis (Frade and Barde, 1998), we also investigated whether macrophages invade the epibranchial placodes. Multiparametric three-dimensional reconstructions of cellular events that occur simultaneously in the developing central and peripheral nervous system provide the groundwork for future molecular analyses.

Materials and methods

Animals

Embryos of the tree shrew *Tupaia belangeri* (Scandentia, average gestation period: 43.7 days, Kuhn and Schwaier, 1973), were collected at the German Primate Center (DPZ), Göttingen, and at the Battelle-Institute, Frankfurt/Main, for unrelated projects of the former Sonderforschungsbereich 89 (Cardiology). In accordance with German law, pregnant *Tupaia belangeri* were killed by intraperitoneal injection of an overdose of pentobarbitone sodium (Nembutal), arterially perfused with Macrodex and 0.15% procaine hydrochloride (Novocain), and fixed with 4% glutaraldehyde/3% paraformaldehyde in phosphate buffer (pH 7.3). Embryos from embryonic days 12 to 19 were embedded and sectioned as specified in Table 1. All embryos used for three-dimensional reconstructions were embedded in Araldite (Serva, Heidelberg, Germany), and completely serially sectioned at 1 μm. Consecutive sections were alternately placed on two sets of slides. Sections of the "working series" (Knabe et al., 2002) were stained with Heidenhain's hematoxylin (Romeis, 1989). Sections of the "reference series" remained unstained and, for reasons detailed below, provided external fiducials for the realignment procedure (Knabe et al., 2002). In previous work, 12- to 16-day-old embryos of our collection were classified according to five arbitrary phases of optic cup formation (Knabe and Kuhn, 1998, 1999; Knabe et al., 2000, 2002). This classification and the designation of each embryo by numbers that indicate the ontogenetic day and an alphabetic order of the embryos of each day were maintained and expanded in the present work:

Phase 1: V-shaped optic evagination
Phase 2: Optic vesicle
Phase 3: Onset of the invagination of the optic vesicle
Phase 4: Advanced invagination
Phase 5: Far advanced invagination/optic fissure
Phase 6: Onset of optic fissure closure

Table 1
Embryos of *Tupaia belangeri* used to investigate epibranchial placodes

Number of embryo in the collection	Age (days) and designation of each embryo in the text	Fixation, embedding, thickness of sections, staining
1396D/C	12a	G/P, A, 2 μm, H
1396D/B	12b	G/P, A, 2 μm, H
DPZ 754/5B	13a	G/P, A, 1 μm, H
1566/C	13b	B, Pa, 7 μm, HE
196/A	13c	B, Pa, 7 μm, HE
1566/B	13d	G/P, A, 1 μm, A/M
DPZ 948/8A	**13e**	G/P, A, 1 μm, H
DPZ 948/1B	13f	G/P, A, 1 μm, H
1284/A	13g	B, Pa, 7 μm, HE
DPZ 754/1A	**13h**	G/P, A, 1 μm, H
DPZ 870/11A	14a	G/P, A, 1 μm, H
DPZ 870/9B	**14b**	G/P, A, 1 μm, H
DPZ 870/12C	14c	G/P, A, 1 μm, H
198/A	14e	F, A, 2 μm, H
198/C	14g	B, Pa, 10 μm, HW/A
962/C	14h	G/P, A, 2 μm, A/M
962/D	14i	G/P, Pa, 7 μm, HE
DPZ 623/9B	**15a**	G/P, A, 1 μm, H
DPZ 743/4B	15b	G/P, GMA, 3 μm, HE
DPZ 743/1A	**15c**	G/P, A, 1 μm, H
DPZ 1384/A	15d	G/P, A, 1 μm, H
1778	15e	B, Pa, 7 μm, HE
386/4A	16a	G/P, Ep, 2 μm, H
166/A	16b	B, Pa, 8 μm, HE
166/B	16c	B, Pa, 7 μm, HE
DPZ 5061/C	**16d**	G/P, A, 1 μm, H
DPZ 10721	16e	B, Pa, 7 μm, HE
1760/A	**17a**	G/P, A, 1 μm, H
DPZ 730/1A	18a	B, GMA, 3 μm, HE
16/A	18b	F, Pa, 7 μm, HE
614/A	19a	B, Pa, 7 μm, HE
DPZ 880/B	19b	B, Pa, 7 μm, A/N

A, Araldite; A/M, Azur II/methylene blue; A/N, Alcian blue/nuclear fast red; B, Bouin's solution; DPZ, German primate center, Göttingen; E, eosin; Ep, Epon; F, formaldehyde; G, glutaraldehyde; GMA, glycolmethacrylate (Kulzer); H, hematoxylin (Heidenhain); HW/A, hematoxylin (Weigert)/azophloxin; P, paraformaldehyde; Pa, paraffin; bold embryo designation, 3-D reconstructed embryo.

Three-dimensional reconstruction

Serial sections were scanned at intervals of 8 μm with the image acquisition system "Huge Image" (Knabe et al., 2002; Süss et al., 2002). This system combines a digital camera (Axiocam HR, Zeiss, Göttingen, Germany), the motorized z-drive of a light microscope (Axioskop 2 MOT, Zeiss), and the motorized x- and y-drives of a scanning table (Märzhäuser, Wetzlar, Germany). All components were connected via interfaces to a PC that was equipped with two 350 MHz CPUs (Pentium II, Intel, Leixlip, Ireland), 56 GB hard disk memory, 640 MB working memory, an accelerated graphics port device with 16 MB memory (Viper TNT, Diamond, Santa Clara, USA) and Windows 2000 (Microsoft, Berlin, Germany). Complete serial sections were scanned line-by-line with the ×100-objective (oil immersion). The resulting small images (650 × 515 pixels) that corresponded to individual fields of view of the camera were automatically assembled to one "huge image" (0.134 μm/pixel; approximately 190000 dpi) with the help of MosaiX (KS400, Zeiss). "Huge images" of complete sections were saved as 8 bit greyscale tiff (tagged image file format)-files. Three-dimensional reconstructions were performed on two PCs with graphics tablets (Intuos A3, Wacom, Krefeld, Germany). The first PC was equipped with a 1.2 GHz CPU (Athlon, AMD GmbH, München, Germany), 200 GB hard disk memory (5T040H4 and 6E040L0, Maxtor EMEA, Massy Cedex, France, and WD1200BB, Western Digital, Lake Forest, USA), 1.5 GB SD-RAM, and an accelerated graphics port device with 64 MB memory (PowerColor Geforce2 Ti, Astra Datentechnik GmbH, Hurth, Germany). The second PC was equipped with a 3.0 GHz CPU (Pentium 4, Intel), 200 GB hard disk memory (6Y080M0 Maxtor EMEA, and WD1200BB, Western Digital), 2.0 GB DDR-RAM, and an accelerated graphics port device with 128 MB DDR memory (Gigacube Radeon 9600 Pro, Info-Tek Corp, Hsin-Chu, Taiwan). Operating systems were Windows 2000 or Windows XP (Microsoft). For histological and cytological analysis, "huge images" were imported to AutoCAD 2000i (Autodesk GmbH, München, Germany). Cellular events, placodal thickenings, and large embryonic contours were manually vectorized (Knabe et al., 2002). Consecutive sections were realigned by creating "hybrid sections" that combined vectorized anatomical data from sections of the working series with vectorized contours of the embedding block taken from corresponding sections of the reference series (for details, see Knabe et al., 2002). In two cases (embryos 16d, 17a), consecutive vectorized sections were realigned by best-fit of the embryonic contours (Süss et al., 2002). Triangulation algorithms modified from Boissonnat (1988) were used to generate meshwires for all large embryonic surfaces (Brunnett et al., 2003).

Diagnosis of cellular events

Semithin sections stained with Heidenhain's hematoxylin (Romeis, 1989) provided good conditions to identify apoptotic cells, mitotic cells, macrophages, and delaminating placodal cells (Fig. 1). According to Sanders and Wride (1995), Knabe and Kuhn (1998, 1999), Goping et al. (1999) and Häcker (2000), structural criteria used to detect apoptotic cells include (1) that single apoptotic cells are scattered among viable ones, (2) that sharply defined rings of condensed chromatin are found at the periphery of the nucleus, (3) that nuclei disassemble into fragments, (4) that apoptotic cells are reorganized into apoptotic bodies, and (5) that strongly stained and sharply delineated apoptotic bodies are incorporated in viable neuroepithelial cells or macrophages. Structural diagnosis of apoptotic cells/bodies in semithin sections as well as in sections from paraffin-embedded embryos (Figs. 1A–C) was proven by reacting representative adjacent sections with the TUNEL method

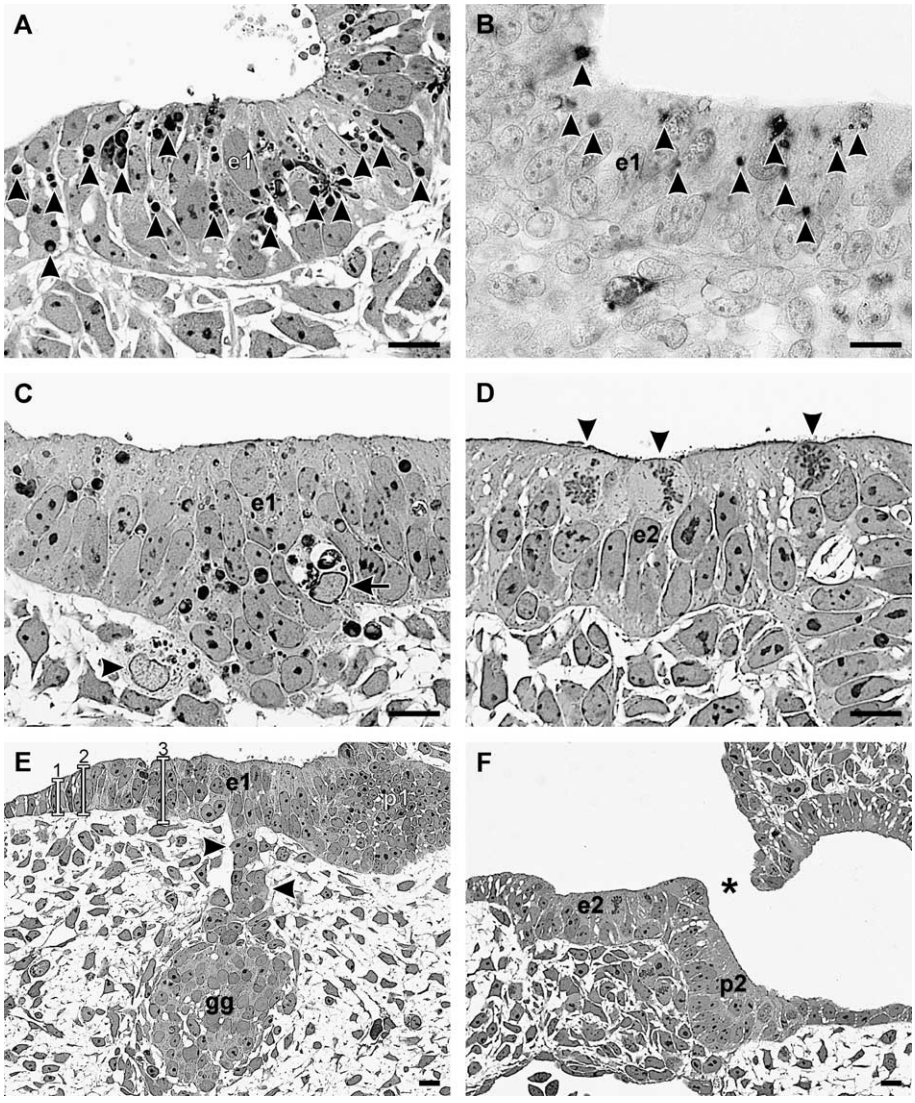

Fig. 1. Cytological diagnosis in hematoxylin-stained semithin sections (1 μm) of Araldite-embedded (A, C–F) and thick sections (7 μm) of paraffin-embedded (B) embryos, *Tupaia belangeri*. (A) Apoptotic cells/bodies (some marked by arrowheads), phase 6 embryo 17a, (B) TUNEL (Terminal Deoxynucleotidyl Transferase-Mediated dUTP Nick End-Labeling)-labeled apoptotic cells/bodies (arrowheads), phase 5 embryo 16e, (C) macrophages with incorporated apoptotic bodies found within (arrow) and adjacent (arrowhead) to epibranchial placodes, phase 5 embryo 16d, and (D) mitotic cells (arrowheads), phase 4 embryo 15c. (E) Streams of delaminating placodal cells (arrowheads), and classification used for 3-D reconstructions of vertically cut ectodermal thickenings: grade 1 (1: "at least one row of cylindrical epithelium"), grade 2 (2: "at least two rows of pseudostratified epithelium"), grade 3 (3: "at least three rows of pseudostratified epithelium"), phase 4 embryo 15c. (F) Perforation (asterisk) of branchial membrane 2, phase 3 embryo 15a, left side. e1, e2, epibranchial placodes 1, 2; gg, geniculate ganglion; p1, p2, pharyngeal pouches 1, 2. Scale bars = 10 μm.

(Terminal Deoxynucleotidyl Transferase-Mediated dUTP Nick End-Labeling): Concentrations of apoptotic cells in the developing brain and in the surface ectoderm are equally well identified in routinely stained or TUNEL-labeled sections (Fig. 7 in Knabe et al., 2004, also for TUNEL-labeling protocol). Spherical meshwire surfaces used to visualize apoptotic bodies (2 to 6 μm: Sanders and Wride, 1995) do not exceed real apoptotic bodies in diameter (Süss et al., 2002). Since serial sections were included in our reconstructions at intervals of 8 μm, apoptotic cells were not numerically overrepresented (Süss et al., 2002).

Macrophages reveal an indented or angular nucleus, abundant foamy cytoplasm, and finger-like pseudopodia. In fixed preparations, a distinct halo separates macrophages from neighboring other cells (Cuadros et al., 1991, 1993; Martín-Partido and Navascués, 1990; Moujahid et al., 1996). Structural diagnosis of macrophages in semithin sections (Fig. 1C) was previously proven by labeling representative other sections with the *Griffonia simplicifolia* Isolectin-B_4 (Knabe and Kuhn, 1999).

Mitotic figures were located and counted irrespective of the orientation of the mitotic cleavage plane. According to Chan et al. (2002), a significant loss of mitotic figures has been observed in insufficiently fixed material. In contrast, mitotic figures are well preserved in perfused animals (Chan et al., 2002, present work: Fig. 1D). To demonstrate regional

differences in the density of mitotic cells, the distribution of all mitotic cells in the ectoderm caudal to branchial membrane 1 was analyzed. Additionally, hot spots of proliferation were determined in standardized lateral views of three-dimensionally reconstructed embryos. Mitotic cells that were separated by the arbitrarily defined distance of less than 25 μm were grouped in individual high rate proliferating zones. "Hot spots" that contained only two mitotic cells were excluded from the evaluation.

Criteria used to identify single or streams of delaminating placodal cells in semithin sections (Fig. 1E) included (1) retained continuity with the placode, (2) protrusion of cytoplasm and parts of the nucleus beyond the level of adjacent placodal cells in two consecutive sections, and (3) absence of an intact basal lamina. Isolated neuroblasts caught in positions intermediate between the placode and the developing ganglion were separately counted.

To identify developing epibranchial placodes, we have arbitrarily defined and separately reconstructed three grades of the thickened surface ectoderm. Only embryos which, to the most possible extent, provided vertically cut regions of interest were chosen for three-dimensional reconstructions. In the single serial section, thickenings were classified as belonging to "grade 1" with at least one row of cylindrical epithelium, "grade 2" with at least two rows of pseudostratified epithelium, or "grade 3" with at least three rows of epithelial cells (Fig. 1E). Consequently, grade 1 zones encompassed grade 2 and grade 3 zones.

Apoptotic bodies, mitotic cells, macrophages, and delaminating cells in the epibranchial placodes were counted in standardized lateral views of reconstructed embryos from six developmental phases. To determine counts per unit of volume, the length and the height of grade 3-defined epibranchial placodes 1 and 2 and, due to the late appearance of grade 3 thickenings, grade 2- and grade 3-defined epibranchial placode 3 were measured. The mean thickness of grade 2 and grade 3 zones was approximated to 20 and 30 μm, respectively.

Photomicrographs (Fig. 1) were acquired with the image acquisition system "Huge Image". To reduce background staining, a "shading correction" was performed in KS400 (Zeiss). Images were imported to Photo-Paint (Corel GmbH), and contrast and sharpness were slightly enhanced using "unsharp mask" and "contrast enhancement" tools.

Results

Morphogenesis of epibranchial placodes

In the phase 1 embryo (Figs. 2A, B), the V-shaped optic evagination communicates with the amniotic sac via the anterior neuroporus. In all other parts of the brain, the neural folds are fused or in the process of fusion. In the transiently segmented hindbrain, neural crest cells delaminate from rhombomeres 1, 2, and more pronounced, 4 and 6. Adjacent to rhombomeres 2 and 4, segregated streams of neural crest cells migrate to the branchial arches 1 and 2, respectively. At the transition of the branchial arches 1 and 2, pharyngeal pouch 1 is attached to the surface ectoderm, and here, will participate in the formation of branchial membrane 1. One single grade 1 zone of thickened surface ectoderm (see Materials and methods, Fig. 1E) extends from the developing branchial membrane 1 to the caudal border of the branchial anlagen. This zone encompasses two grade 2 zones. The first one combines the otic placode and the tongue-like branch that extends from the otic placode to branchial arch 2. This branch includes the future position of epibranchial placode 1. The second grade 2 zone foreshadows epibranchial placode 2.

In the phase 2 embryo (Figs. 2C, D), the lumen of the globular optic vesicle is connected to the forebrain ventricle. The neural tube is closed in all parts of the brain. Streams of migrating neural crest cells extend from the mesenchyme adjacent to rhombomeres 2, 4, and 6 to the branchial arches 1, 2, and 3, respectively. At the site of contact between the pharyngeal pouch 1 and the surface ectoderm, endoderm- and ectoderm-derived epithelial cells merge in the developing branchial membrane 1. At the transition of branchial arch 2 and developing branchial arch 3, pharyngeal pouch 2 is attached to the surface ectoderm, and contributes to the formation of branchial membrane 2. Grade 1 zones are partly lost on branchial membranes 1 and 2 as well as in the strip of ectoderm that descends caudally adjacent to the otic pit and terminates on branchial arch 2. The preexisting grade 2 zone that combined the otic placode and developing epibranchial placode 1 persists. Grade 2 zones in the future positions of the epibranchial placodes 1 and 2 are broadened. Narrow grade 3 zones foreshadow epibranchial placode 1 and, right side, epibranchial placode 2. Focal high-grade thickenings are also found in the ectoderm ventral to the pharyngeal pouches 1 and 2, respectively. These ventral thickenings may represent anlagen of "hypobranchial placodes" (Schlosser, 2003, but see Discussion).

In the phase 3 embryo (Figs. 2E, F), initial thickening of the lateral wall of the optic vesicle signifies the onset of optic cup formation. A short optic stalk connects the optic cup to the forebrain. Developing N.VII contacts rhombomere 4, and terminates close to the dorsal tip of pharyngeal pouch 1. The combined proximal anlagen of Nn.IX/X are found adjacent to rhombomeres 6/7. The two nerves terminate close to the dorsal tips of the pharyngeal pouches 2 and 3, respectively. Rudiments of the geniculate ganglion as well as of the distal ganglia IX (petrosal) and X (nodose) have developed. For the first time, anlagen of Nn.XI and XII are discernible. Pharyngeal pouches 1 to 3 are attached to the surface ectoderm. Grade 1 zones disappear (1) from the surface ectoderm that overlays the detached otic vesicle, (2) from the caudal two thirds of branchial arch 2, (3) completely from branchial membranes 1 and 2, and (4) partly from branchial arch 3 and branchial

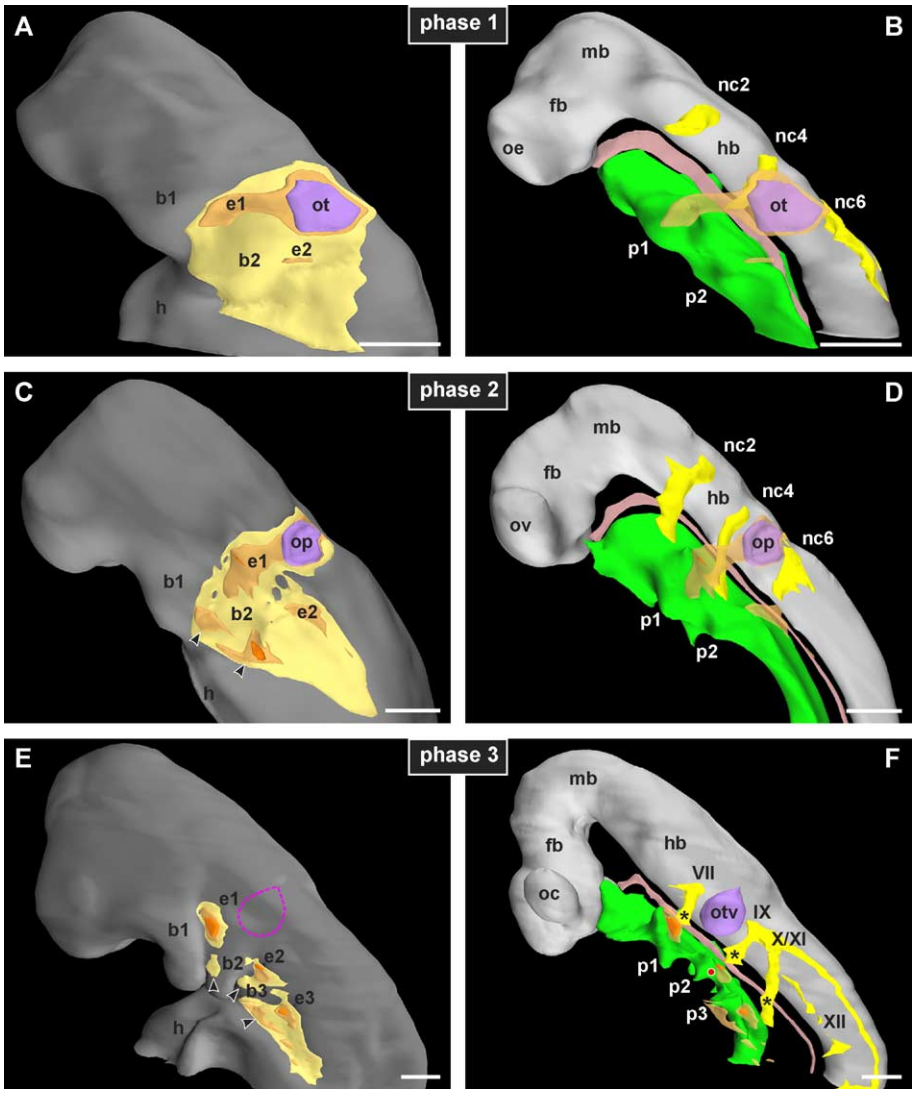

Fig. 2. Morphogenesis of epibranchial placodes, *Tupaia belangeri*, phases 1 to 3. 3-D reconstructions show surface ectoderm (grey), neuroepithelium (light grey), ectodermal thickenings: grade 1 (light yellow), grade 2 (light orange), grade 3 (orange), neural crest streams (yellow), otic anlage (violet), projection of otic vesicle on surface ectoderm (dashed violet), endoderm (green), and notochord (light brown). (A, C, and E) Regression of the grade 1 zone is paralleled by the appearance of high-grade thickenings in the future positions of the epibranchial placodes. (B, D, and F) Epibranchial placodes develop upon contact with pharyngeal pouches in a rostrocaudal sequence. Note ectodermal thickenings (arrowheads in C, E) ventral to the pharyngeal pouches, and rudiments of the three epibranchial ganglia (asterisks in F). (F) Branchial membrane 2 is perforated (red dot) in phase 3. b1, b2, b3, branchial arches 1, 2, 3; cranial nerves VII, facial; IX, glossopharyngeal; X, vagus; XI, accessory; XII, hypoglossal; e1, e2, e3, epibranchial placodes 1, 2, 3; fb, forebrain; h, heart; hb, hindbrain; mb, midbrain; nc2, nc4, nc6, crest cells adjacent to rhombomeres 2, 4, 6; ot, otic placode; op, otic pit; otv, otic vesicle; oe, optic evagination; ov, optic vesicle; oc, optic cup; p1, p2, p3, pharyngeal pouches 1, 2, 3. Scale bars = 200 μm.

membrane 3. Separate grade 2 and grade 3 zones mark the three epibranchial placodes. As an exception, grade 3 ectoderm is absent from epibranchial placode 3 on the right side of the embryonic body. An isolated grade 1 zone persists ventral to the pharyngeal pouch 1. Grade 1 ectoderm that encompasses epibranchial placode 2 continuously extends to the position ventral to the pharyngeal pouch 2. Focal high-grade thickenings ventral to the pharyngeal pouch 3 share one single grade 1 zone with epibranchial placode 3.

In the phase 4 embryo (Figs. 3A, B), the thickness of the developing retina is increased and the lumen of the optic ventricle is reduced, compared with phase 3. Consequently, phase 4 represents an advanced stage of optic cup formation. Other advanced features of phase 4 include the initial segregation of Nn.IX and X adjacent to the hindbrain wall, the stronger roots of N.XII, and the increased size of the geniculate, petrosal, and nodose ganglia. Pharyngeal pouch 4 approaches the surface ectoderm. All three grades of ectodermal thickening concur in defining epibranchial placode 1. Dorsal parts of epibranchial placode 2 are represented by almost congruent grade 2 and grade 3 zones. Isolated grade 2 zones which, in phase 3, foreshadowed epibranchial placode 3, unite and enlarge on the branchial arches 4 and 6. Additionally, right more than left side, a grade 2 zone arises in the dorsal position intermediate

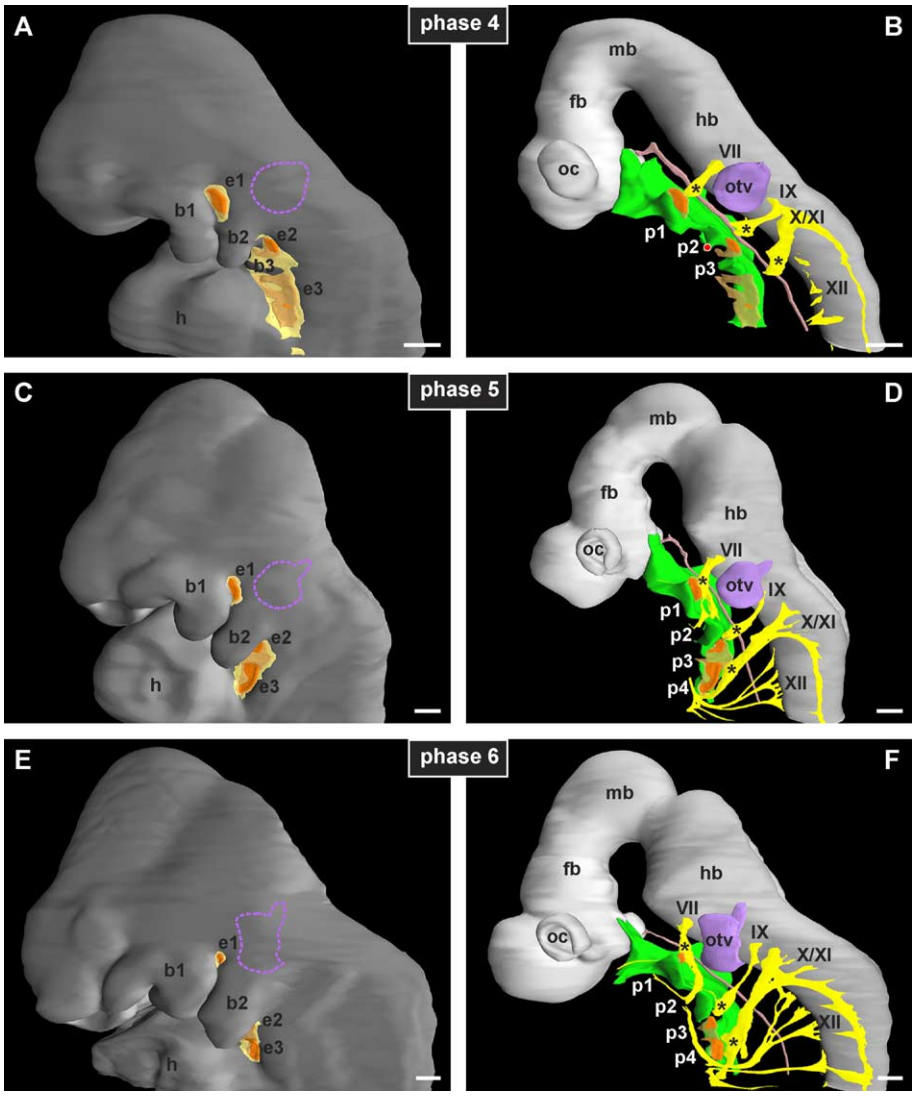

Fig. 3. Morphogenesis of epibranchial placodes, *Tupaia belangeri*, phases 4 to 6. 3-D reconstructions show surface ectoderm (grey), neuroepithelium (light grey), ectodermal thickenings: grade 1 (light yellow), grade 2 (light orange), grade 3 (orange), otic anlage (violet), projection of otic vesicle on surface ectoderm (dashed violet), cranial nerves (yellow), endoderm (green), and notochord (light brown). Epibranchial placodes "mature" in a rostrocaudal sequence (A, C, and E), and reside adjacent to pharyngeal pouches 1, 2, and 3, respectively (B, D, and F). Note the three epibranchial ganglia (asterisks in B, D, and F). Branchial membrane 2 is perforated (red dot) in phase 4 (B). b1, b2, b3, branchial arches 1, 2, 3; cranial nerves VII, facial; IX, glossopharyngeal; X, vagus; XI, accessory; XII, hypoglossal; e1, e2, e3, epibranchial placodes 1, 2, 3; fb, forebrain; h, heart; hb, hindbrain; mb, midbrain; oc, optic cup; otv, otic vesicle; p1, p2, p3, p4, pharyngeal pouches 1, 2, 3, 4. Scale bars = 200 μm.

between the epibranchial placodes 2 and 3. Ectodermal thickenings ventral to the pharyngeal pouches 2 and 3 persist. These ventral thickenings share at least grade 1 zones with the epibranchial placodes 2 and 3, respectively.

In the phase 5 embryo (Figs. 3C, D), optic cup formation is far advanced. The optic fissure is discernible. Compared with phase 4, boundaries between the three major divisions of the brain are more pronounced. The endolymphatic duct emerges from the dorsomedial region of the otic vesicle. Ascending spinal and future intracranial roots of N.XI are discernible. The roots of N.XII join to a single nerve. Branchial arch 2 starts overgrowing branchial arch 3. Branchial membrane 2 is drawn inward. Epibranchial placode 1 slightly decreases in size, whereas epibranchial placode 2 elongates in the ventral direction. Grade 3 ectoderm marks the fully formed epibranchial placode 3. Except for a narrow grade 1 zone found on branchial arch 3, one single grade 2 zone coats the branchial arches 3, 4, and 6.

In the phase 6 embryo (Figs. 3E, F), closure of the optic fissure has started. Branches of Nn.VII, IX, and X (not detailed here) have grown further towards their peripheral targets. Nn.IX and X separately enter the hindbrain. Branchial arch 2 is increased in size and, in the lateral view, obscures epibranchial placode 2. Epibranchial placode 1 is markedly shrunken. With respect to size and position, the epibranchial placodes 2 and 3 are essentially unchanged. Perforations of the branchial membranes are

always found in branchial membrane 2 (phases 3 to 5: Figs. 1F, 2F and 3B), but variably left side (embryos 15a, 15c), right side (16a, 16d), or on both sides of the embryonic body (15e, 16b, 16c).

Patterns of cellular events in epibranchial placodes

Criteria used to identify apoptotic and mitotic cells (Figs. 4 and 5) as well as macrophages and delaminating placodal cells (Fig. 6) are shown in Fig. 1 (for details, see Materials and methods). Table 2 demonstrates that reconstructed embryos share major sites of apoptosis with 21 other serially sectioned embryos (phases 1 to 6). Hot spots of proliferation as well as major sites of apoptosis and delamination of placodal cells found on left and right sides of the reconstructed embryos were unified in summary schemes (Fig. 7).

In phase 1 (Figs. 4A, B and 7A, A′), higher numbers of mitotic cells are present in the single branchial grade 1 zone compared with the adjacent non-thickened ectoderm. On

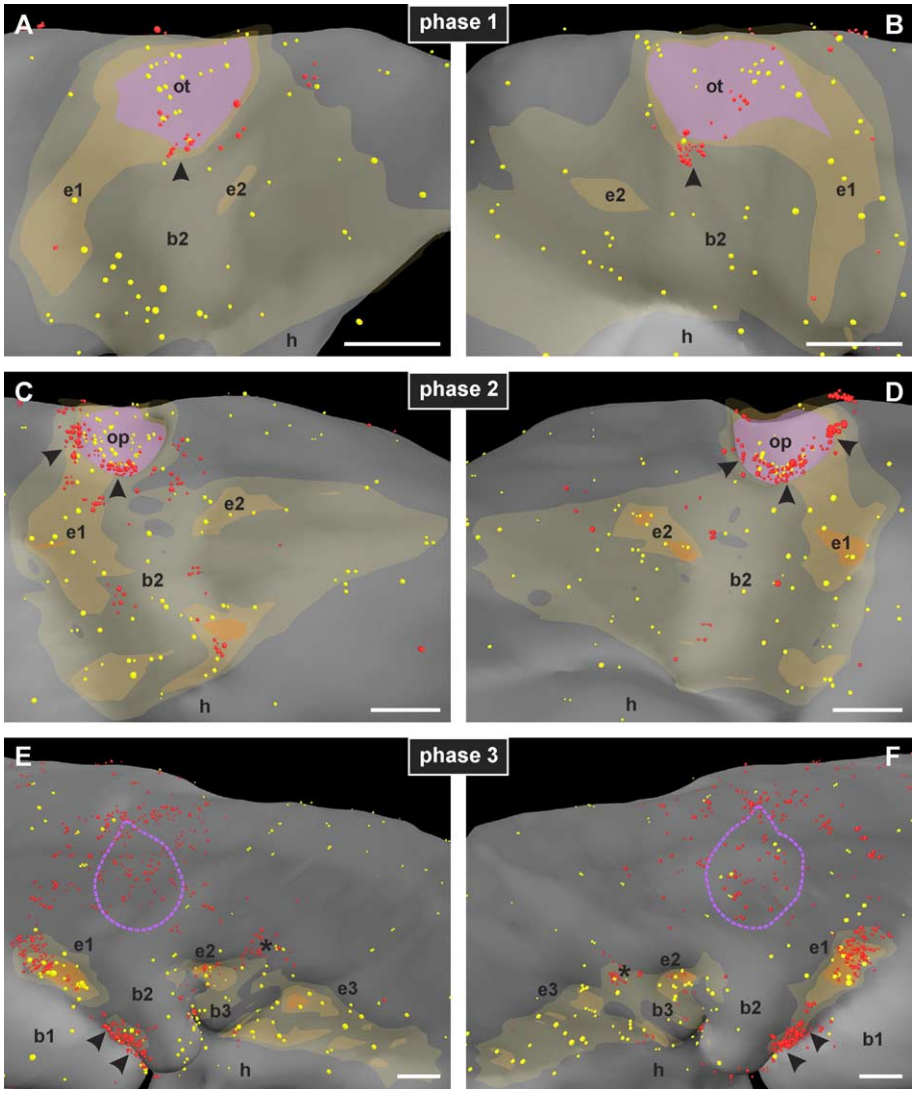

Fig. 4. Apoptosis and proliferation in epibranchial placodes, *Tupaia belangeri*, phases 1 to 3. (A, C, and E) Left side of the embryonic body, (B, D, and F) right side. 3-D reconstructions show surface ectoderm (grey), ectodermal thickenings: grade 1 (light yellow), grade 2 (light orange), grade 3 (orange), otic anlage (violet), projection of otic vesicle on surface ectoderm (dashed violet), apoptotic cells/bodies (red dots, 1.75-fold radius), and mitotic cells (yellow dots). (A, B) Phase 1: Hot spots of proliferation are found in the otic placode and, more randomly scattered, ventrally on branchial arch 2 as well as right side (B) in developing epibranchial placode 1 and ventrally adjacent to developing epibranchial placode 2. Note focal apoptosis (arrowheads) at the ventrocaudal margin of the otic placode. (C, D) Phase 2: mitotic cells are concentrated in the otic pit, and in developing epibranchial placodes 1 and 2. A sickle-shaped band of apoptotic cells (arrowheads) demarcates the otic placode ventrally. (E, F) Phase 3: Apoptotic cells are concentrated (1) in the ectoderm overlaying the otic vesicle as well as rostrally, dorsally, and caudally adjacent to this position, (2) in dorsal parts of epibranchial placodes 1 and 2, (3) in the grade 1 zone ventrally adjacent to epibranchial placode 1 (arrowheads), and (4) dorsally intermediate between epibranchial placodes 2 and 3 (asterisks). Concentrations of mitotic cells are centered on all three epibranchial placodes. For detailed description, see text. b1, b2, b3, branchial arches 1, 2, 3; e1, e2, e3, epibranchial placodes 1, 2, 3; h, heart; ot, otic placode; op, otic pit. Scale bars = 100 μm.

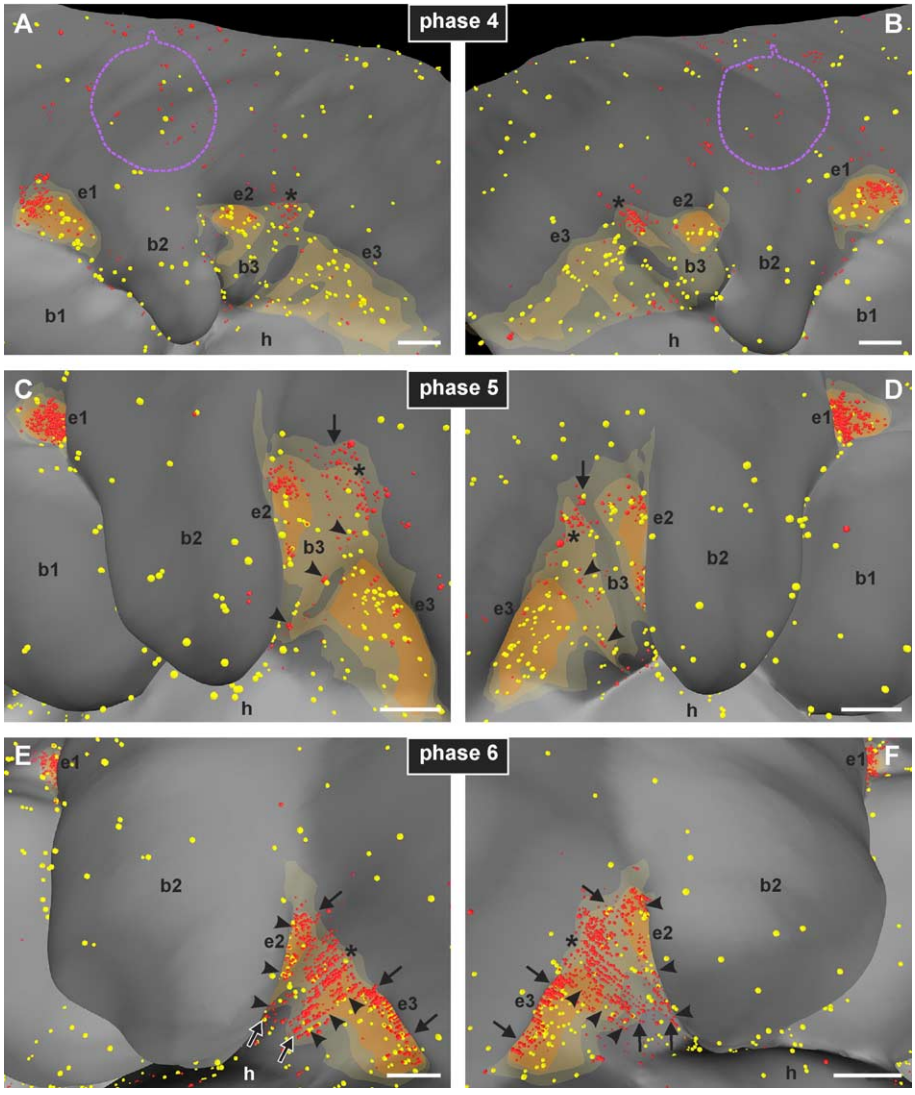

Fig. 5. Apoptosis and proliferation in epibranchial placodes, *Tupaia belangeri*, phases 4 to 6. (A, C, and E) Left side of the embryonic body, (B, D, and F) right side. 3-D reconstructions show surface ectoderm (grey), ectodermal thickenings: grade 1 (light yellow), grade 2 (light orange), grade 3 (orange), projection of otic vesicle on surface ectoderm (dashed violet), apoptotic cells/bodies (red dots, 2-fold radius), mitotic cells (yellow dots, 1.25-fold radius). (A, B) Phase 4: hot spots of proliferation are present in all three epibranchial placodes. Apoptotic cells are found (1) dorsally in epibranchial placode 1, (2) initially in dorsal parts of epibranchial placodes 2 and 3, (3) in the ectoderm overlaying the otic vesicle as well as rostrally, dorsally, and caudally adjacent to this position, and (4) dorsally intermediate between epibranchial placodes 2 and 3 (asterisks). (C, D) Phase 5: high numbers of mitotic cells persist in epibranchial placodes 1, 2, and 3. Concentrations of apoptotic cells are found in epibranchial placodes 1 (throughout), 2 (dorsal and ventral parts) and, initially, 3 (dorsal). Focal apoptosis persists at the dorsal transition of epibranchial placodes 2 and 3 (asterisks, compare with A, B), but expands rostrally (arrow) and ventrally down on branchial arch 3 (arrowheads). (E, F) Phase 6: hot spots of proliferation reside in epibranchial placodes 2 and 3. Apoptotic cells are concentrated throughout epibranchial placode 1 (completely shown in Fig. 6J). Two horizontal (arrows) and two vertical bands of apoptotic cells (arrowheads) encompass apoptosis in epibranchial placodes 2 (throughout) and 3 (dorsal half), and the preexisting apoptotic focus found at the dorsal transition of epibranchial placodes 2 and 3 (asterisks). For detailed description, see text. b1, b2, b3, branchial arches 1, 2, 3; e1, e2, e3, epibranchial placodes 1, 2, 3; h, heart. Scale bars = 100 μm.

left and right sides of the embryonic body, hot spots of proliferation are found in the otic placode. Other concentrations of mitotic cells tend to predominate in rostral parts of the grade 1 zone, but are observed unilaterally: dorsally adjacent to the future position of epibranchial placode 1 (right side), ventrocaudally adjacent to the grade 2 zone that combines the otic placode and epibranchial placode 1 (left), in other parts of branchial arch 2, and ventrally adjacent to the developing epibranchial placode 2 (right). Apoptotic cells are concentrated at the ventrocaudal margin of the otic placode.

In phase 2 (Figs. 4C, D and 7B, B′), high rate proliferating zones are present in the entire otic pit as well as in dorsal parts of the developing epibranchial placodes 1 and 2, respectively. Other hot spots of proliferation are concentrated on branchial arch 2 as well as in the grade 2 zones ventral to the pharyngeal pouches 1 and 2 (left). A few single mitotic cells are scattered on the caudal branchial

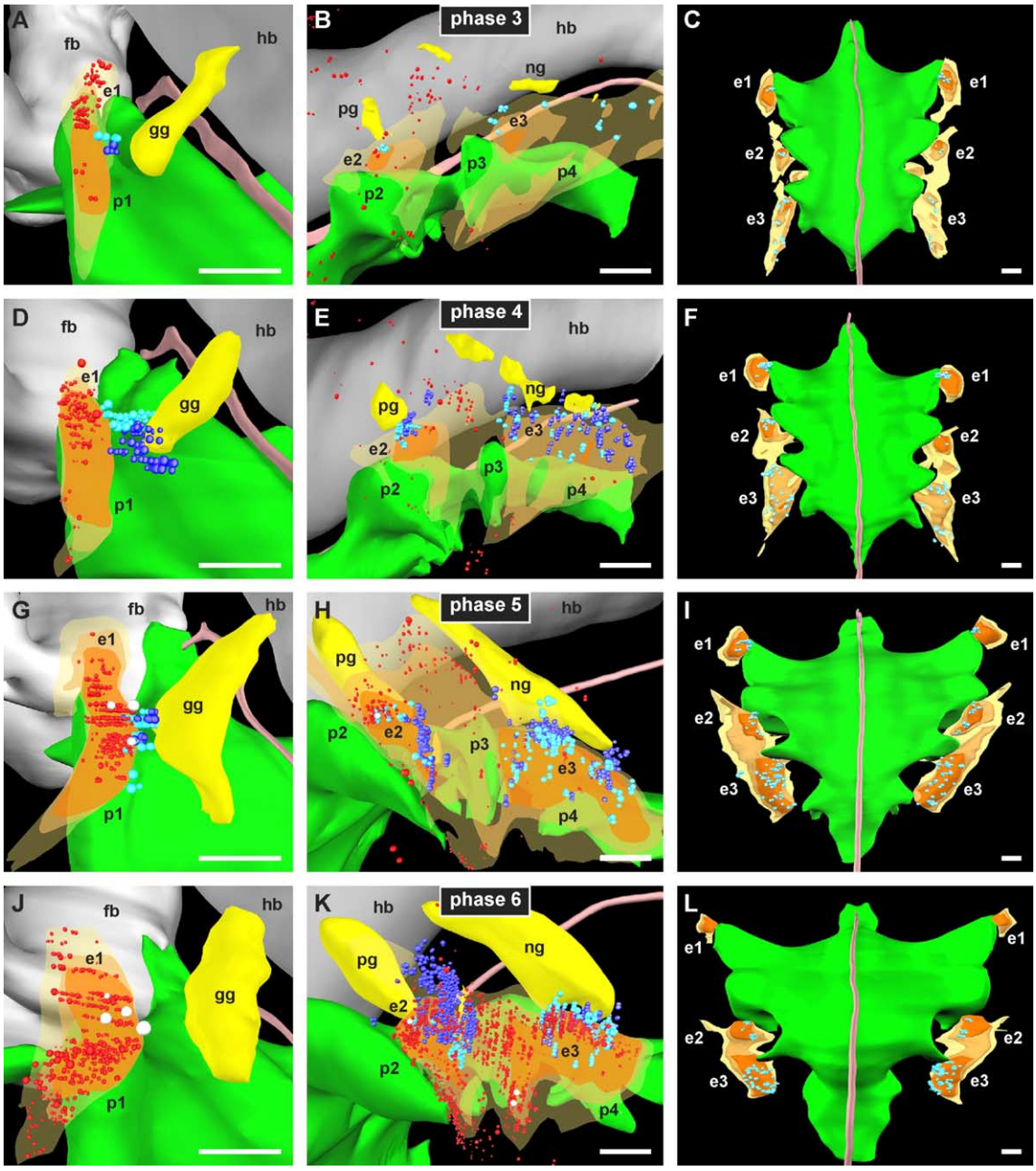

Fig. 6. Apoptosis and delamination in epibranchial placodes, *Tupaia belangeri*, phases 3 (A–C), 4 (D–F), 5 (G–I), and 6 (J–L): Oblique lateral views (A, D: mirror-imaged from right side, G, and J), lateral views (B, E, H, and K), dorsal views (C, F, I, and L). 3-D reconstructions show neuroepithelium (grey), ectodermal thickenings: grade 1 (light yellow), grade 2 (light orange), grade 3 (orange), endoderm (green), notochord (light brown), apoptotic cells/bodies (red dots, 2-fold radius), macrophages (white dots, 1.1-fold radius), delaminating placodal cells (light blue dots, 1.5-fold radius), migrating placodal cells (blue dots, 1.5-fold radius). Epibranchial placode 1: dorsal onset of apoptosis and delamination (A), dorsoventral progression of apoptosis and delamination (D, G), and ceased delamination with apoptosis throughout the placode (J). Epibranchial placode 2: apoptosis and delamination start dorsally (B, E) and, later, extend ventrad (H, K). Epibranchial placode 3: dorsal onset of delamination (B) precedes dorsal onset of apoptosis (E, H, and K). (C, F, I, and L) Patterns of delamination in three pairs of epibranchial placodes, phases 3 to 6. Note delamination from distinct rostral and caudal sites in epibranchial placode 3 on one or both sides of the embryonic body (C, F, and I). e1, e2, e3, epibranchial placodes 1, 2, 3; gg, geniculate ganglion; pg, petrosal ganglion; ng, nodose ganglion; p1, p2, p3, p4, pharyngeal pouches 1, 2, 3, 4. Scale bars = 100 μm.

arches. A sickle-shaped band of apoptotic cells demarcates the ventral margin of the otic pit. This band helps to "separate" the otic pit from epibranchial placode 1 that share one single grade 2 zone except for in the embryos 13b and 13d. Other groups of apoptotic cells are found in the grade 2 zone intermediate between the otic pit and epibranchial placode 1 (left side), and between the otic pit and epibranchial placode 2 in regressing parts of the grade 1 zone. Additionally, apoptotic foci are present on branchial arch 2, on branchial membrane 2 (left), in the grade 2 zone

Table 2
Patterns of apoptosis observed during the morphogenesis of epibranchial placodes

Phase	Embryo	Ot: ventrocaudal margin (focus)	Op: ventral margin (band)	Ecto over Otv	E1:		Ecto ventrally adjacent to E1	E2:		Ecto dorsally between E2 and E3 (focus)	E3:		Ecto with E2 and E3 (complex-shaped band)
					dorsal half	ventral half		dorsal half	ventral half		dorsal half	ventral half	
1	13a	–, ++											
	13h	++, ++											
2	12a		+, ++		–, –	–, –		–, –	–, –				
	12b		+, +		–, –	–, –		–, –	–, –				
	13b		++, ++		+, –	–, –		–, –	–, –				
	13c		+, –		–, –	–, –		–, –	–, –				
	13d		++, ++		–, –	–, –		–, –	–, –				
	13e		++, ++		–, –	–, –		–, –	–, –	+, –			
	13f	–, +	+, –		–, –	–, –		–, –	–, –				
	13g		++, ++		–, –	–, –		–, –	–, –				
3	14a			–, +	–, +	–, –	–, –	–, –	–, –	++, –	–, –	–, –	–, –
	14b			+, +	+, +	–, –	–, –	–, –	–, –	++, ++	–, –	–, –	–, –
	14c			+, +	+, +	–, –	+, +	+, +	–, –	+, +	–, –	–, –	–, –
	15a			++, ++	++, ++	–, +	++, ++	+, +	–, –	++, ++	–, –	–, –	–, –
4	14e			++, ++	++, ++	–, –	–, –	–, –	–, –	++, ++	–, –	–, –	–, –
	14g			–, –	++, ++	–, –	–, –	+, +	–, –	++, ++	–, –	–, –	–, –
	14h			–, –	++, ++	–, –	+, ++	+, +	–, –	+, +	–, –	–, –	–, –
	14i			+, +	+, +	–, –	++, –	+, +	–, –	–, –	–, –	–, –	–, –
	15b			+, +	++, ++	–, –	–, –	–, +	–, –	+, +	–, –	–, –	–, –
	15c			+, +	++, ++	–, +	+, +	–, +	–, –	++, ++	–, –	–, –	–, –
	15d			+, +	+, +	–, –	+, +	++, –	–, –	+, +	–, –	–, –	–, –
5	15e			–, –	++, ++	+, –	–, –	++, +	+, –	+, ++	–, –	–, –	–, –
	16a			–, –	++, ++	+, +	–, –	++, +	++, +	++, ++	–, –	–, –	–, –
	16b			–, –	++, ++	++, ++	–, –	++, ++	+, +	+, ++	+, +	–, –	–, –
	16c			–, –	++, ++	+, ++	–, –	++, ++	+, +	++, ++	+, +	–, –	+, +
	16d			–, –	++, ++	++, ++	–, –	++, ++	+, +	++, ++	+, +	–, –	+, +
6	**17a**			–, –	++, ++	++, ++	–, –	++, ++	++, ++	++, ++	++, ++	–, –	++, ++

++, high numbers of apoptotic cells; +, low to moderate numbers of apoptotic cells; –, absence of apoptotic concentrations; E, epibranchial placode; Ecto, ectoderm; Ot, otic placode; Op, otic pit; Otv, otic vesicle; bold embryo number, 3-D reconstructed embryo; numbers of apoptotic cells were separately given for right and left sides of the embryonic body.

ventrally adjacent to branchial membrane 2 (left), and in the grade 1 zone dorsocaudally adjacent to epibranchial placode 2 (right).

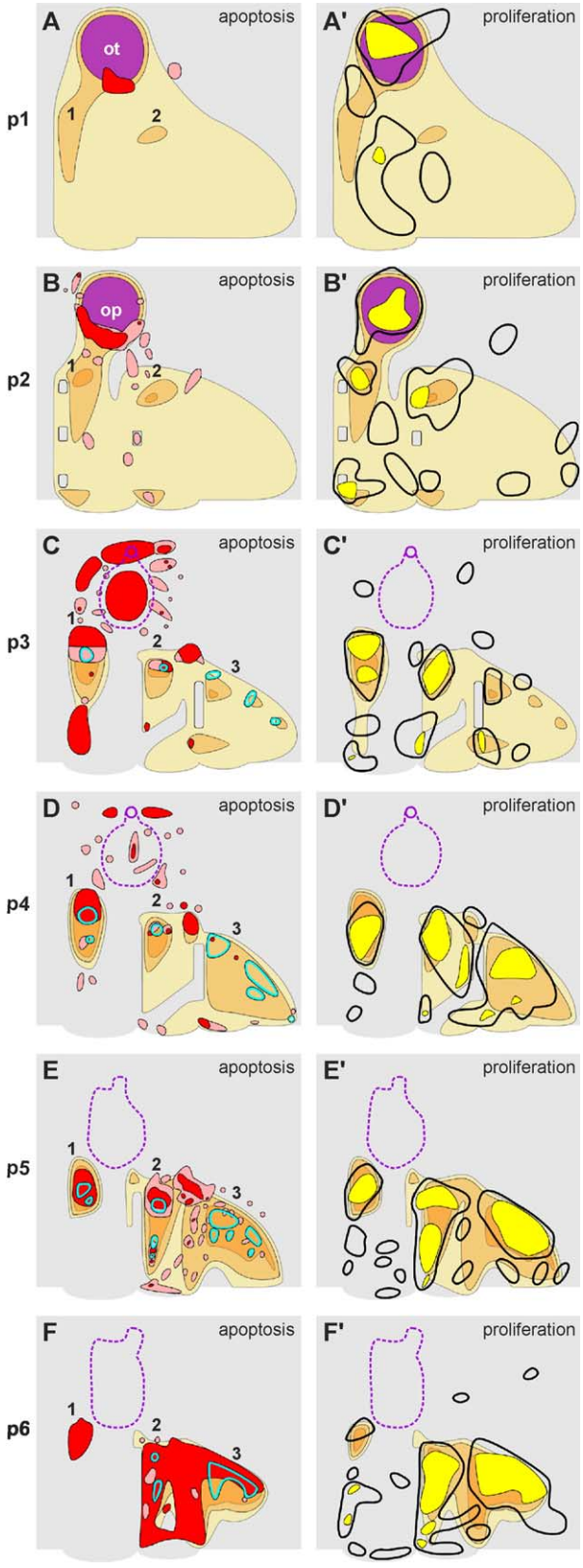

In phase 3 (Figs. 4E, F and 7C, C′), high rate proliferating zones are found in dorsal and ventral parts of the epibranchial placodes 1 and 2 as well as dorsorostrally in the developing epibranchial placode 3 (right side). Other groups of mitotic cells are concentrated in thickened parts of the ectoderm ventral to the pharyngeal pouches 1, 2, and 3, respectively. Paralleling the further regression of grade 1 ectoderm, hot spots of proliferation start to disappear from caudal parts of branchial arch 2. Apoptotic cells are concentrated in the undetached dorsal tip of the otic vesicle, and in the thin ectoderm that overlays the otic vesicle as well as rostrally, dorsally, and caudally adjacent to this area. Other groups of apoptotic cells are found between the former position of the otic placode and the epibranchial placodes 1 and 2, respectively, in thinned out parts of preexisting grade 1 and grade 2 zones (phases 1 and 2). Concentrations of apoptotic cells also reside in dorsal parts of the epibranchial placodes 1 and 2, in the grade 1 zone ventrally adjacent to epibranchial placode 1, and in the dorsal position intermediate between the epibranchial placodes 2 and 3. Additionally, apoptotic foci are present in the thickened ectoderm ventral to the pharyngeal pouches 2 and 3. In embryo 14b, a triangular-shaped field of apoptotic ectodermal cells coats rhombomeres 6/7. In the dorsal halves of epibranchial placode 1 and, less pronounced, epibranchial placode 2, precursor cells delaminate from zones with overlapping concentrations of apoptotic and mitotic cells (Figs. 6A–C and 7C). In dorsal parts of epibranchial placode 3, some few cells emigrate from distinct rostral and caudal positions. That, in fact, earliest precursor cells delaminate from the epibranchial placodes in phase 3 was confirmed in the embryos 14a, 14b, and 14c.

In phase 4 (Figs. 5A, B and 7D, D′), high-rate proliferating zones are noted in dorsal and ventral parts of all three epibranchial placodes. Other groups of mitotic cells are found ventrally adjacent to epibranchial placode 1, and in the thickened ectoderm ventral to the pharyngeal pouches 2 and 3, respectively. The continued decrease in proliferation observed on branchial arch 2 is paralleled by the

Fig. 7. Patterns of apoptosis (A–F), proliferation (A′–F′), and precursor cell delamination (C–F) in epibranchial placodes, 3-D reconstructed embryos, *Tupaia belangeri*, phases 1 to 6 (p1–p6). Diagrams are lateral views unified from left and right sides of the embryonic body, and show thin surface ectoderm (grey), ectodermal thickenings: grade 1 (light yellow), grade 2 (light orange), grade 3 (orange), otic placode or pit (violet), detached otic vesicle (dashed violet), undetached dorsal tip of otic vesicle (violet circle), concentrations of apoptotic cells on one (light red) or both sides (red) of the embryonic body, hot spots of proliferation on one (thick black lines) or both sides (yellow) of the embryonic body, and delaminating placodal cells (light blue). Three pairs of epibranchial placodes develop in a rostrocaudal sequence. Apoptosis helps to "individualize" the otic placode and epibranchial placode 1 as well as the epibranchial placodes 1, 2, and 3. Simultaneously, high-rate proliferating zones arise in the developing epibranchial placodes. Rostrocaudal waves of proliferation, apoptosis, and delamination proceed from dorsal to ventral parts of the definitive placodes. For detailed description, see text. 1, 2, 3, epibranchial placodes 1, 2, 3; ot, otic placode; op, otic pit.

increase in the number and size of hot spots on the caudal branchial arches. Compared with phase 3, concentrations of apoptotic cells persist, albeit with lower numbers, in the ectoderm that overlays the otic vesicle and immediately round about this latter position. Other concentrations of apoptotic cells are found in the dorsal half of epibranchial placode 1, and in the dorsal position intermediate between the epibranchial placodes 2 and 3. Some few apoptotic cells are scattered in the ventral half of epibranchial placode 1 (left side), and in dorsal parts of the epibranchial placodes 2 and 3. Additionally, apoptotic foci reside ventrally adjacent to epibranchial placode 1, in the thin ectoderm ventral to pharyngeal pouch 2, and in the grade 1 zone ventral to pharyngeal pouch 3. Increased numbers of emigrating precursor cells are found in all three epibranchial placodes (Figs. 6D–F and 7D). These cells delaminate from zones with overlapping concentrations of apoptotic and mitotic cells in the dorsal halves of the epibranchial placodes 1 and 2, and less pronounced in the ventral half of epibranchial placode 1. In dorsal parts of epibranchial placode 3, precursor cells emigrate from distinct rostral and caudal positions (left side) or right, along the rostrocaudal length of the placode.

In phase 5 (Figs. 5C, D and 7E, E′), high rate proliferating zones reside throughout the epibranchial placodes 1, 2, and 3. Compared with phase 4, these hot spots are more centered on the ventrally elongated epibranchial placode 2 as well as on the grade 3 defined epibranchial placode 3. Other hot spots of proliferation are scattered ventrally on branchial arch 2 and, slightly more pronounced, in ventral parts of the caudal branchial arches. High-rate proliferating zones colocalize with concentrations of apoptotic cells almost throughout epibranchial placode 1, in dorsal and ventral parts of epibranchial placode 2, and initially, in dorsorostral parts of epibranchial placode 3. Concentrations of apoptotic cells are also found dorsally intermediate between the epibranchial placodes 2 and 3. From this latter position, groups of apoptotic cells extend band-like towards epibranchial placode 2 as well as ventrally down the caudal half of branchial arch 3. Additionally, apoptotic foci are present within and adjacent to thickened parts of the ectoderm ventral to the pharyngeal pouches 2 and 3. In the epibranchial placodes 1 and 2, precursor cells emigrate from zones with overlapping concentrations of apoptotic and mitotic cells. Compared with phase 4, delamination has shifted from dorsal to ventral parts in epibranchial placode 1, persists in the dorsal third of epibranchial placode 2, and starts in ventral parts of epibranchial placode 2 (Figs. 6G–I and 7E). Dorsally, epibranchial placode 3 releases high numbers of precursor cells from two (left side) or three (right) positions. Some few cells also delaminate from ventral and rostralmost parts of the placode. That, in a mammal, epibranchial placode 3 arises from isolated rostral and caudal thickenings (phases 3 to 6) and releases precursor cells from distinct rostral and caudal positions (phases 3 to 5) reminds on the fact that two to six vagal epibranchial placodes are found in lampreys, fish, amphibia, or birds (Baker and Bronner-Fraser, 2001).

In phase 6 (Figs. 5E, F and 7F, F′), high-rate proliferating zones completely coat the epibranchial placodes 2 and 3. Compared with phase 5, proliferation in epibranchial placode 1 is markedly reduced (left side) or almost absent (right). Again, other hot spots of proliferation are scattered ventrally on branchial arch 2 and, more pronounced, on the caudal branchial arches including thickened parts of the ectoderm ventral to the pharyngeal pouches 2 and 3. Apoptotic cells are found throughout epibranchial placode 1 (also see Fig. 6J). Other concentrations of apoptotic cells overlap high-rate proliferating zones in the entire epibranchial placode 2, and in the dorsal half of epibranchial placode 3. Apoptosis in epibranchial placode 2 belongs to the vertical band of apoptotic cells which, adjacent to branchial membrane 2, extends from dorsalmost to ventralmost parts of branchial arch 3. A second vertical band descends rostrally adjacent to branchial membrane 3. The two vertical bands are connected by two horizontal bands of apoptotic cells that traverse branchial arch 3 dorsally and ventrally. The broader dorsal horizontal band encompasses the apoptotic focus which, from phase 3 onwards, resides intermediate between the epibranchial placodes 2 and 3. Caudally, this dorsal horizontal band of apoptotic cells passes through the approximate dorsal half of epibranchial placode 3. Delamination ceases in epibranchial placode 1 (Figs. 6J–L and 7F). Precursor cells emigrate from zones with overlapping concentrations of apoptotic and mitotic cells in the dorsal and ventral thirds of epibranchial placode 2 as well as in the entire dorsal third of epibranchial placode 3. Additionally, precursor cells delaminate from ventrorostral and ventrocaudal parts of epibranchial placode 3, in the absence of neighboring apoptotic cells.

Apoptotic bodies, mitotic cells, macrophages, and delaminating cells were counted in the epibranchial placodes of reconstructed embryos (Table 3). In phase 3,

Table 3
Cellular events counted in epibranchial placodes

Cellular event	Placode	Phase 2 **13e**	Phase 3 **15a**	Phase 4 **15c**	Phase 5 **16d**	Phase 6 **17a**
Apo	E1	0	2.91	4.03	14.87	24.97
	E2	0	1.16	0.47	2.51	7.71
	E3		0.01	0.02	0.16	7.17
Del	E1	0	0.58	1.76	1.21	0
	E2	0	1.39	1.07	1.85	1.78
	E3		0.51	0.69	1.96	2.38
Mit	E1	1.02	0.55	0.47	0.43	0.68
	E2	0.77	0.75	0.77	0.52	0.60
	E3		0.50	0.55	0.59	0.79
Mac	E1	0	0	0	0.10	0.36
	E2	0	0	0	0.02	0.04
	E3		0	0	0	0.02

Apo, apoptotic bodies; Del, delaminating placodal cells; E, epibranchial placode; Mit, mitotic cells; Mac, macrophages; bold embryo number, 3-D reconstructed embryo; counts given per unit volume ×10 000.

delamination starts in all three epibranchial placodes. Compared with epibranchial placode 1, maximum numbers of precursor cells delaminate from the epibranchial placodes 2 and 3 with a delay. In epibranchial placodes 1 and 2, the onset of delamination coincides with the onset of apoptosis. In epibranchial placode 3, delamination precedes apoptosis by at least one phase. Features shared by all three epibranchial placodes (Fig. 7, Table 3) include (1) the onset of increased local proliferation prior to (epibranchial placodes 1 and 2) or, at least, concurrently with the onset of delamination (epibranchial placode 3), (2) the onset of proliferation and, with a short delay, apoptosis and delamination in dorsal parts of the definitive placode, (3) the progression of proliferation, apoptosis, and delamination from dorsal to ventral parts of the placode, (4) the marked increase in the number of apoptotic bodies per unit of volume during ongoing delamination, (5) the persistence of increased local proliferation until delamination ceases, and (6) the late immigration of macrophages. Macrophages invade epibranchial placode 1 (embryos 16a, 16d) and, with lower numbers, epibranchial placode 2 (16d) in phase 5 (Figs. 1C and 6G, H). In phase 6, higher numbers of macrophages are found in the two placodes (Figs. 6J, K). Additionally, macrophages are noted in the ectoderm that coats branchial arch 3 as well as in epibranchial placode 3. Generally, macrophages colocalize with massive concentrations of apoptotic cells.

The fate of all three epibranchial placodes was determined in embryos 18a, 18b, 19a, and 19b. 18a reveals high numbers of apoptotic cells throughout the pit-shaped epibranchial placode 1. Delamination has ceased. All other embryos demonstrate grade 1 or grade 2 zones in the former position of epibranchial placode 1. On embryonic day 18, apoptotic cells are also concentrated throughout epibranchial placode 2. Precursor cells either delaminate from dorsal and ventral halves of the placode (18a) or are absent (18b). In 19a and 19b, remnants of epibranchial placode 2 are no longer discernible. Concerning epibranchial placode 3, 18a closely resembles the reconstructed phase 6 embryo (Figs. 5E, F, 6J–L and 7F, F′). In 18b, apoptotic cells are concentrated throughout the deeply invaginated placode with highest numbers in its ventral parts. Compared with 18a, delamination is decreased. In 19a and 19b, again, large-scale apoptosis is found in the remnants of the placode and delamination has ceased.

Discussion

The present work demonstrates that spatially and temporally regulated sequences of apoptotic and proliferative events pass through the epibranchial placodes of *Tupaia belangeri*. Multiparametric three-dimensional reconstructions suggest distinct functions for apoptosis in developing, mature, and regressing epibranchial placodes. First, apoptosis in the thickened surface ectoderm that surrounds the emerging placodes helps to establish three pairs of epibranchial placodes in a rostrocaudal sequence. Second, apoptosis contributes to the selection of premigratory placodal cells destined to populate the epibranchial ganglia. Third, apoptosis eliminates the remnants of epibranchial placodes. In *Tupaia*, rhombomere-specific apoptosis of premigratory neural crest cells (phases 1, 2: Knabe et al., 2004) precedes dorsoventrally directed apoptosis in the epibranchial placodes during the peak-period of precursor cell delamination (phase 3 onwards). Since rhombencephalic neural crest and epibranchial placodes successively provide cells for the geniculate, petrosal, and nodose ganglia, apoptosis of precursor cells in the two distant sources might be regulated by coordinated signaling.

Cranial neural crest cells are not the prime movers for branchial arch patterning. Instead, key processes during the organization of the branchial arches depend on interactions with the pharyngeal endoderm (Graham et al., 2004): In chick embryos, epibranchial placodes are induced by BMP-7 that is expressed in the pharyngeal pouches at the sites of contact with the surface ectoderm (Begbie et al., 1999). Correspondingly, in *Tupaia*, epibranchial placodes arise upon contact with the pharyngeal pouches 1, 2, and 3 in a rostrocaudal sequence. We have identified developing epibranchial placodes by three-dimensionally reconstructing three arbitrary grades of thickened ectoderm. As has been reported for embryonic chick, mice, and human embryos (Baker and Bronner-Fraser, 2000; Bartelmez and Evans, 1926; D'Amico-Martel and Noden, 1983; Ishii et al., 2001; Müller and O'Rahilly, 1988; Verwoerd and van Oostrom, 1979), epibranchial placodes in *Tupaia* develop step-by-step within more extended areas of thickened ectoderm. According to Bartelmez and Evans (1926), epibranchial placodes arise from the thickened branchial ectoderm by secondary thickening. Alternatively, preexisting thickenings may persist in the position of epibranchial placodes, while neighboring parts of the ectoderm become thinned out (Ishii et al., 2001; Müller and O'Rahilly, 1988; Verwoerd and van Oostrom, 1979). The two apparently different views are not irreconcilable. In *Tupaia*, apoptotic events adjacent to the emerging placodes as well as placode-bound hot spots of proliferation assist in the "shaping" of epibranchial placodes. Thus, grade 2 thickened ectoderm transiently encompasses epibranchial placode 1 and the otic placode. Combined anlagen of the two placodes also exist in *Xenopus laevis*, embryonic chick, laboratory mice, and human embryos (Atwell, 1930; Ishii et al., 2001; Schlosser and Ahrens, 2004; Verwoerd and van Oostrom, 1979). In *Tupaia*, a sickle-shaped apoptotic band then springs up at the ventral margin of the otic placode, and apoptosis thins out ectoderm at the transition of the otic placode and epibranchial placodes 1 and 2, respectively. Consequently, epibranchial placodes 1 and 2 are demarcated dorsally. These findings suggest that concentrations of apoptotic cells found at the ventral margin of the otic placode may not only promote its invagination to the otic pit (Hirata and Hall, 2000). In

Tupaia, the dorsal apoptotic demarcation of epibranchial placode 1 is complemented by the apoptotic thinning of ectoderm ventrocaudally adjacent to the placode as well as in the ectoderm that overlays the detached otic vesicle. Simultaneously, proliferation increases in the epibranchial placodes, and grade 3 ectoderm signifies the definitive positions of epibranchial placodes 1 and 2. From phase 3 onwards, apoptotic cells are concentrated at the dorsal transition of the epibranchial placodes 2 and 3. In phases 5 and 6, this focus of apoptotic cells merges into a much more extended, complex-shaped apoptotic field which helps to individualize the proliferating post-otic epibranchial placodes. We conclude that, in *Tupaia*, spatiotemporally controlled apoptotic and proliferative events contribute to the morphogenesis of all three epibranchial placodes. However, observed concentrations of apoptotic cells may neither necessarily nor exclusively separate strictly localized placodal primordia. In chick embryos, extensive migrations and rearrangements of heterogenous precursor cells in the ectoderm precede and accompany the development of morphologically distinct otic and epibranchial placodes (Streit, 2002). Consequently, apoptosis found adjacent to the emerging placodes in *Tupaia* may eliminate migrating precursor cells. Future studies are needed to determine the identity of the observed apoptotic cells, and to clarify how balanced apoptotic and proliferative events in the anlagen of epibranchial placodes are regulated.

In 1999, a novel type of neurogenic placode was described in anurans (Schlosser and Northcutt, 2000; Schlosser et al., 1999). These hypobranchial placodes are situated in the ectoderm ventral to the pharyngeal pouches 2 and 3, arise from a broader primordial thickening that includes the epibranchial placodes, and produce neurons destined to populate hypobranchial ganglia of unknown function (Schlosser, 2003). So far, hypobranchial placodes have been reported in anurans and urodeles, but not in zebrafish, chick, or mouse embryos (for review, see Schlosser, 2003). Interestingly, ectodermal thickenings ventral to the pharyngeal pouches 1, 2, and 3 were found in *Tupaia*. These thickenings colocalize with ventral foci of mitosis and apoptosis that topographically correspond closely to the hypobranchial placodes described in frogs (Schlosser, 2003). Consequently, our findings suggest that homologues of hypobranchial placodes may exist in *Tupaia*, but are completely eliminated by apoptosis. Future molecular analyses of the developing epibranchial placodes in *Tupaia* will help to clarify whether observed thickenings of the ventral ectoderm that, like epibranchial placodes, arise from a common primordial thickening have any relevance as neurogenic placodes.

Epibranchial placodes and branchial membranes develop in parallel. Whether perforations of branchial membranes observed in reptilia, birds, and mammals represent physiological openings or artifacts, and whether these perforations result from focally increased cell death is under debate. According to Mangold et al. (1981), extreme thinning and the presence of "degenerated" cells predispose branchial membrane 2 to perforate in embryonic rats and mice. Conversely, the fact that perforations of branchial membrane 1 are rare (Mangold et al., 1981) or absent (Poelmann et al., 1985) has been attributed to the scarcity of apoptotic cells compared with mitotic cells (Poelmann et al., 1985). In embryonic chick, "cellular reorganization" (Waterman, 1985) or "differential cell proliferation" (Miller et al., 1993) rather than apoptosis cause perforations of the branchial membranes. In the studied embryos of *Tupaia*, perforations were invariably located in branchial membrane 2 on one or both sides of the embryonic body. Correspondingly, perforations of branchial membrane 2 are frequently found in *Lacerta vivipara* as well as in chick, bovine, ovine, mouse, rat, and human embryos (Froriep, 1885; Liessner, 1888; Mangold et al., 1981; Politzer and Hann, 1935; Waterman, 1985). In *Tupaia*, these perforations never colocalized with concentrations of apoptotic cells. Consequently, our findings do not support the view that cell death contributes to the formation of "branchial clefts" in mammals (Mangold et al., 1981).

In the developing nervous system, macrophages and "non-professional phagocytes" eliminate apoptotic cells (Knabe et al., 2000; Rabinovitch, 1995). Macrophages also can induce apoptosis, for example, by releasing nerve growth factor that activates the p75 neurotrophin receptor (Frade and Barde, 1998). The presence of macrophages in epibranchial placodes has never been documented. However, in rat embryos, macrophages have been observed in the mesenchyme adjacent to epibranchial placode 1 (Adelmann, 1925). In *Tupaia*, macrophages invade "bands" of apoptotic cells in the forebrain and eyes from embryonic day 14 onwards (Knabe and Kuhn, 1999; Knabe et al., 2000). The present findings demonstrate that macrophages are late immigrants in all three epibranchial placodes and, generally, invade preexisting sites of large-scale apoptosis. Consequently, macrophages help to eliminate apoptotic cells, but do not significantly contribute to the induction of apoptosis in the epibranchial placodes of *Tupaia*.

A systematic three-dimensional analysis of the sequence of apoptotic and proliferative events in epibranchial placodes has not been published, so far. Adelmann (1925) mentioned that, in rat embryos, the number of pycnotic cells in epibranchial placode 1 increases with time. Correspondingly, in laboratory mice, epibranchial placodes reveal higher numbers of apoptotic cells in 33 somite embryos compared with 18 somite embryos (Sulik et al., 1987). According to Batten (1957), the late appearance of pycnotic cells in the invaginated epibranchial placode 1 of sheep embryos coincides with a decrease in the number of mitotic cells. The presence of pycnotic cells in the epibranchial placodes of human embryos either has been stated (Theiler, 1949) or is likely from inspection of the provided figures (Ilies, 1967). Our three-dimensional reconstructions demonstrate that, in *Tupaia*, rostrocaudal waves of apoptosis and proliferation

pass through the three pairs of epibranchial placodes and, thus, parallel their order of maturation. The three epibranchial placodes share major patterns of the studied cellular events: (1) Proliferation and, with a short delay, apoptosis start dorsally and, later, extend to ventral parts of the placode, (2) the dorsal onset of apoptosis coincides with or is slightly preceded (epibranchial placode 3) by the dorsal onset of precursor cell delamination, (3) paralleling the sequence of apoptotic and proliferative events, delamination starts dorsally and extends to ventral parts of the placode, (4) precursor cells delaminate from sites with overlapping concentrations of apoptotic and proliferative cells, (5) delamination ceases as soon as large scale apoptosis resides in the entire placode, and (6) apoptosis persists throughout the regressing placode. We conclude that, in the epibranchial placodes of *Tupaia*, spatially and temporally regulated apoptotic and proliferative events help to select premigratory precursor cells destined to populate the geniculate, petrosal and nodose ganglia. Thereafter, apoptosis contributes to the elimination of the placodes in a rostrocaudal sequence.

Acknowledgments

We thank Dr. Marek Vanco, Technical University Chemnitz, for help with the three-dimensional reconstructions, and Irmgard Weiß for technical assistance.

This work was supported by the Deutsche Forschungsgemeinschaft (KN 525/1-1, KN 525/1-2, BR 1185/4-1, and former Sonderforschungsbereich 89: Cardiology).

References

Adelmann, H.B., 1925. The development of the neural folds and cranial ganglia of the rat. J. Comp. Neurol. 39, 19–171.

Atwell, W.J., 1930. A human embryo with 17 pairs of somites. Contrib. Embryol. Carnegie Inst. 21, 1–24.

Baker, C.V.H., Bronner-Fraser, M., 2000. Establishing neuronal identity in vertebrate neurogenic placodes. Development 127, 3045–3056.

Baker, C.V.H., Bronner-Fraser, M., 2001. Vertebrate cranial placodes I. Embryonic induction. Dev. Biol. 232, 1–61.

Bartelmez, G.W., Evans, H.M., 1926. Development of the human embryo during the period of somite formation, including embryos with 2 to 16 pairs of somites. Contrib. Embryol. Carnegie Inst. 17, 1–67.

Batten, E.H., 1957. The behavior of the epibranchial placode of the facial nerve in the sheep. J. Comp. Neurol. 108, 393–420.

Begbie, J., Graham, A., 2001. Integration between the epibranchial placodes and the hindbrain. Science 294, 595–598.

Begbie, J., Brunet, J.F., Rubenstein, J.L., Graham, A., 1999. Induction of the epibranchial placodes. Development 126, 895–902.

Boissonnat, J.D., 1988. Shape reconstruction from planar cross sections. Comput. Vis. Graph. Image Process. 44, 1–29.

Brunnett, G., Vanco, M., Haller, C., Washausen, S., Kuhn, H.-J., Knabe, W., 2003. Visualization of cross sectional data for morphogenetic studies. In: Dittrich, K., König, W., Oberweis, A., Rannenberg, K., Wahlster, W. (Eds.), Proceedings GI Workshop "Visualisierung in der Bioinformatik", Lecture Notes in Informatics vol. 34. Köllen, Bonn, pp. 354–359.

Chan, W.Y., Lorke, D.E., Tiu, S.C., Yew, D.T., 2002. Proliferation and apoptosis in the developing human neocortex. Anat. Rec. 267, 261–276.

Cuadros, M.A., García-Martín, M., Martin, C., Ríos, A., 1991. Haemopoietic phagocytes in the early differentiating avian retina. J. Anat. 177, 145–158.

Cuadros, M.A., Martin, C., Coltey, P., Almendros, A., Navascués, J., 1993. First appearance, distribution, and origin of macrophages in the early development of the avian central nervous system. J. Comp. Neurol. 330, 113–129.

D'Amico-Martel, A., Noden, D.M., 1983. Contributions of placodal and neural crest cells to avian cranial peripheral ganglia. Am. J. Anat. 166, 445–468.

Dixon, J., Hovanes, K., Shiang, R., Dixon, M.J., 1997. Sequence analysis, identification of evolutionary conserved motifs and expression analysis of murine tcof1 provide further evidence for a potential function for the gene and its human homologue, TCOF1. Hum. Mol. Genet. 6, 727–737.

Dixon, J., Brakebusch, C., Fässler, R., Dixon, M.J., 2000. Increased levels of apoptosis in the prefusion neural folds underlie the craniofacial disorder, Treacher Collins syndrome. Hum. Mol. Genet. 9, 1473–1480.

Frade, J.M., Barde, Y.A., 1998. Microglia-derived nerve growth factor causes cell death in the developing retina. Neuron 20, 35–41.

Froriep, A., 1885. Ueber Anlagen von Sinnesorganen am Facialis, Glossopharyngeus und Vagus, über die genetische Stellung des Vagus zum Hypoglossus, und über die Herkunft der Zungenmusculatur. Arch. Anat. Physiol., 1–55.

Goping, G., Wood, K.A., Sei, Y., Pollard, H.B., 1999. Detection of fragmented DNA in apoptotic cells embedded in LR white: a combined histochemical (LM) and ultrastructural (EM) study. J. Histochem. Cytochem. 47, 561–568.

Graham, A., Heyman, I., Lumsden, A., 1993. Even-numbered rhombomeres control the apoptotic elimination of neural crest cells from odd-numbered rhombomeres in the chick hindbrain. Development 119, 233–245.

Graham, A., Begbie, J., McGonnell, I., 2004. Significance of the cranial neural crest. Dev. Dyn. 229, 5–13.

Häcker, G., 2000. The morphology of apoptosis. Cell Tissue Res. 301, 5–17.

Hamburger, V., Hamilton, H.L., 1951. A series of normal stages in the development of the chick embryo. J. Morphol. 88, 49–92.

Hirata, M., Hall, B.K., 2000. Temporospatial patterns of apoptosis in chick embryos during the morphogenetic period of development. Int. J. Dev. Biol. 44, 757–768.

Ilies, A., 1967. La topographie et la dynamique des zones nécrotiques normales chez l'embryon humain. Rev. Roum. Embryol. Cytol. Ser. Embryol. 4, 51–84.

Ishii, Y., Abu-Elmagd, M., Scotting, P.J., 2001. Sox3 expression defines a common primordium for the epibranchial placodes in chick. Dev. Biol. 236, 344–353.

Knabe, W., Kuhn, H.-J., 1998. Pattern of cell death during optic cup formation in the tree shrew *Tupaia belangeri*. J. Comp. Neurol. 401, 352–366.

Knabe, W., Kuhn, H.-J., 1999. The earliest invasion of macrophages into the developing brain and eye of the tree shrew *Tupaia belangeri*. Anat. Embryol. 200, 393–402.

Knabe, W., Süss, M., Kuhn, H.-J., 2000. The patterns of cell death and of macrophages in the developing forebrain of the tree shrew *Tupaia belangeri*. Anat. Embryol. 201, 157–168.

Knabe, W., Washausen, S., Brunnett, G., Kuhn, H.-J., 2002. Use of "reference series" to realign histological serial sections for three-dimensional reconstructions of the positions of cellular events in the developing brain. J. Neurosci. Methods 121, 169–180.

Knabe, W., Washausen, S., Brunnett, G., Kuhn, H.-J., 2004. Rhombomere-specific patterns of apoptosis in the tree shrew *Tupaia belangeri*. Cell Tissue Res. 316, 1–13.

Kotch, L.E., Sulik, K.K., 1992. Patterns of ethanol-induced cell death in the developing nervous system of mice; neural fold states through the time of anterior neural tube closure. Int. J. Dev. Neurosci. 10, 273–279.

Kuhn, H.-J., Schwaier, A., 1973. Implantation, early placentation, and the chronology of embryogenesis in *Tupaia belangeri*. Anat. Embryol. 142, 315–340.

Lee, S.A., Shen, E.L., Fiser, A., Sali, A., Guo, S., 2003. The zebrafish forkhead transcription factor Foxi1 specifies epibranchial placode-derived sensory neurons. Development 130, 2669–2679.

Liessner, E., 1888. Ein Beitrag zur Kenntnis der Kiemenspalten und ihrer Anlagen bei amnioten Wirbelthieren. Gegenbaurs Morphol. Jahrb. 13, 402–426.

Mangold, U., Dörr, A., Kaufmann, P., 1981. Die Kiemenbogenentwicklung bei Ratte und Maus II. Zur Existenz von Kiemenspalten. Acta Anat. 110, 23–34.

Martín-Partido, G., Navascués, J., 1990. Macrophage-like cells in the presumptive optic pathways in the floor of the diencephalon of the chick embryo. J. Neurocytol. 19, 820–832.

Miller, S.A., Favale, A.M., Knohl, S.J., 1993. Role for differential cell proliferation in perforation and rupture of chick pharyngeal closing plates. Anat. Rec. 237, 408–414.

Moujahid, A., Navascués, J., Marín-Teva, J.L., Cuadros, M.A., 1996. Macrophages during avian optic nerve development: relationship to cell death and differentiation into microglia. Anat. Embryol. 193, 131–144.

Müller, F., O'Rahilly, R., 1988. The development of the human brain from a closed neural tube at stage 13. Anat. Embryol. 177, 203–224.

Poelmann, R.E., Dubois, S.V., Hermsen, C., Smits-van Prooije, A.E., Vermeij-Keers, C., 1985. Cell degeneration and mitosis in the buccopharyngeal and branchial membranes in the mouse embryo. Anat. Embryol. 171, 187–192.

Politzer, G., Hann, F., 1935. Über die Entwicklung der branchiogenen Organe beim Menschen. Z. Anat. Entwicklungsgesch. 104, 670–708.

Rabinovitch, M., 1995. Professional and non-professional phagocytes: an introduction. Trends Cell Biol. 5, 85–87.

Romeis, B., 1989. Heidenhain's hematoxylin. In: Böck, P. (Ed.), Mikroskopische Technik. Urban-Schwarzenberg, Baltimore, pp. 10–100.

Sanders, E.J., Wride, M.A., 1995. Programmed cell death in development. Jeon, K.W., Jarvik, J. International Review of Cytology, vol. 163. Academic Press, London, pp. 105–173.

Schlosser, G., 2002. Development and evolution of lateral line placodes in amphibians I. Development. Zoology 105, 119–146.

Schlosser, G., 2003. Hypobranchial placodes in *Xenopus laevis* give rise to hypobranchial ganglia, a novel type of cranial ganglia. Cell Tissue Res. 312, 21–29.

Schlosser, G., Ahrens, K., 2004. Molecular anatomy of placode development in *Xenopus laevis*. Dev. Biol. 271, 439–466.

Schlosser, G., Northcutt, R.G., 2000. Development of neurogenic placodes in *Xenopus laevis*. J. Comp. Neurol. 418, 121–146.

Schlosser, G., Kintner, C., Northcutt, R.G., 1999. Loss of ectodermal competence for lateral line placode formation in the direct developing frog *Eleutherodactylus coqui*. Dev. Biol. 213, 354–369.

Streit, A., 2002. Extensive cell movements accompany formation of the otic placode. Dev. Biol. 249, 237–254.

Sulik, K.K., Johnston, M.C., Daft, P.A., Russell, W.E., Dehart, D.B., 1986. Fetal alcohol syndrome and DiGeorge anomaly: critical ethanol exposure periods for craniofacial malformations as illustrated in an animal model. Am. J. Med. Genet., Suppl. 2, 97–112.

Sulik, K.K., Johnston, M.C., Smiley, S.J., Speight, H.S., Jarvis, B.E., 1987. Mandibulofacial dysostosis (Treacher Collins syndrome): a new proposal for its pathogenesis. Am. J. Med. Genet. 27, 359–372.

Sulik, K.K., Cook, C.S., Webster, W.S., 1988. Teratogens and craniofacial malformations: relationships to cell death. Development 103, 213–231.

Süss, M., Washausen, S., Kuhn, H.-J., Knabe, W., 2002. High resolution scanning and three-dimensional reconstruction of cellular events in large objects during brain development. J. Neurosci. Methods 113, 147–158.

Theiler, K., 1949. Studien zur Entwicklung der Ganglienleiste: II. Teil. Befunde zur Frühentwicklung der Ganglienleiste beim Menschen. Acta Anat. 8, 96–112.

Verwoerd, C.D.A., van Oostrom, C.G., 1979. Cephalic neural crest and placodes. Adv. Anat. Embryol. Cell Biol. 58, 1–75.

Waterman, R.E., 1985. Formation and perforation of closing plates in the chick embryo. Anat. Rec. 211, 450–457.

Webb, J.F., Noden, D.M., 1993. Ectodermal placodes: contributions to the development of the vertebrate head. Am. Zool. 33, 434–447.

Wendling, O., Dennefeld, C., Chambon, P., Mark, M., 2000. Retinoid signaling is essential for patterning the endoderm of the third and fourth pharyngeal arches. Development 127, 1553–1562.

Wible, J.R., Zeller, U., 1994. Cranial circulation of the pen-tailed tree shrew *Ptilocercus lowii* and relationships of Scandentia. J. Mamm. Evol. 2, 209–230.